

# Reciprocal space engineering with hyperuniform gold metasurfaces

Marta Castro-Lopez,<sup>1</sup> Michele Gaio,<sup>1</sup> Steven Sellers,<sup>2</sup> George Gkantzounis,<sup>2</sup> Marian Florescu,<sup>2,\*</sup> and Riccardo Sapienza<sup>1,†</sup>

<sup>1</sup>*Department of Physics, King's College London, Strand, London WCR 2LS, United Kingdom.*

<sup>2</sup>*Department of Physics, University of Surrey, Guildford, Surrey GU27XH, United Kingdom.*

Hyperuniform geometries feature correlated disordered topologies which follow from a tailored k-space design. Here we study gold plasmonic hyperuniform metasurfaces and we report evidence of the effectiveness of k-space engineering on both light scattering and light emission experiments. The metasurfaces possess interesting directional emission properties which are revealed by momentum spectroscopy as diffraction and fluorescence emission rings at size-specific k-vectors. The opening of these rotational-symmetric patterns scales with the hyperuniform correlation length parameter as predicted via the spectral function method.

Coherent control of optical waves by scattering from 2D nanostructured surfaces is revolutionising the way we shape the wavefront of an incoming light beam, opening new avenues for miniaturised optical components for integrated optical circuits [1], flat display technology [2], and energy harvesting [3, 4]. Metallic surfaces are in particular attractive due to the strong light-matter interaction associated with surface plasmons, enabling diffraction control through plasmonic crystals [5, 6] and metal nano-particle arrays [7, 8], broadband operation and increase of the plasmon mode density [9], enhanced omnidirectional light extraction and coupling [10], broadband absorption [11], fluorescence enhancement [12] and lasing [13, 14], and more recently the realisation of ultra thin lenses [15] and metasurface holograms [16].

Whereas periodic geometries suffer from limited rotational symmetries, aperiodic and disordered topologies, with their richer symmetries and patterns, can lead to superior optical functionalities [8], as in omnidirectional absorption for solar applications [17, 18], scattering-induced light localisation [19] and light extraction from LED/OLED [20]. Moreover, disordered metasurfaces are expected to be more resilient against fabrication imperfection and therefore more apt for technological implementation. Given the vast possible designs of non-periodic topologies, ranging from random to correlated-disordered, their full potential is still to be fully explored.

There exists a general class of disordered systems, called hyperuniform disordered (HuD) photonic structures, which are of particular interest because they exhibit wide and isotropic photonic band gaps [21], rotational symmetry and broadband k-space control, and can be systematically generated through a specific design rule via universal tessellation protocol [22, 23]. Pioneering experiments on photonic HuD systems have explored IR light diffraction in 3D dielectric structures [24], microwave band-gaps formation [25], polarization filtering [26] and random quantum cascade lasers [27]. Theoretical proposals have been put forward for surface enhanced Raman scattering [28], transparency design [29],

high-Q optical cavities and low-loss waveguides [30–32], and microwave photonic circuits [25]. HuD structures fabrication is improving quickly, reaching already the IR range [24] but not yet the visible.

Here, we report visible light scattering and light emission experiments from HuD plasmonic gold metasurfaces. We find that scattering from the metasurfaces is principally directed into an annular angular pattern indicating reciprocal space engineering. Moreover, we investigate directional emission from near-field coupled emitters which, as confirmed by theoretical modelling, is shaped into a ring from the effective band folding into the light cone by scattering processes.

The metasurface design is derived from a stealth hyperuniform point pattern with  $\chi = 0.49$  comprising 4000 points [22] and generated under a periodic boundary condition, for a given average inter-scatterer distance  $a$ . A section of the point pattern, decorated by discs of radius  $0.3a$ , is shown in Fig. 1A. The structure factor of the point pattern is shown in Fig. 1B: the point distribution exhibits significant local structural correlations: the typical exclusion region around  $\mathbf{k} = 0$  which characterizes stealthy hyperuniform patterns and a broad isotropic diffraction maximum peaked around  $ak/2\pi = 1.03$ .

Next, a Delaunay tessellation protocol [22] is performed, obtaining a strictly trivalent continuous network topology (Fig. 1C) with walls of thickness  $0.35a$ . The structure factor of this network is presented in Fig. 1D. The stealthiness of the architecture has been significantly reduced: the diffraction spectrum (Fig. 1D, inset) exhibits low intensity diffuse scattering around  $\mathbf{k} = 0$ , in contrast to the sharp exclusion zone of the simple point pattern (Fig. 1B, inset). Nonetheless, the general form of the point pattern structure factor dominated by a single broad and isotropic resonance around  $ak/2\pi = 1.09$  is reproduced by the network.

Gold metasurfaces were fabricated by electron beam lithography on a glass substrate for various size scaling parameters  $a$ . The samples are of two kind: *pillar-type* samples comprising isolated pentagonal, hexagonal and heptagonal gold pillars (sketched in Fig. 1E and SEM

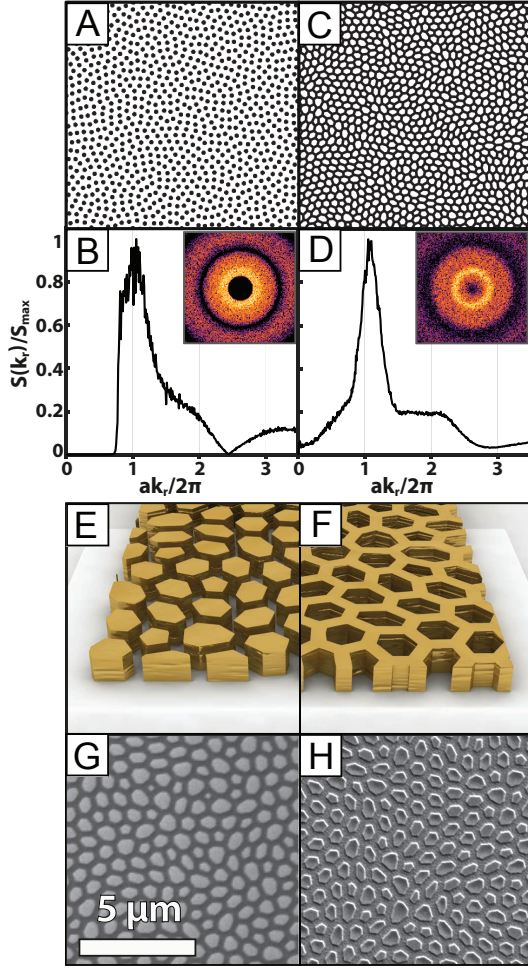


FIG. 1. The initial HuD point pattern (panel A) with  $\chi = 0.49$  presents a structure factor (panel B) with a typical zero around  $\mathbf{k} = 0$  and a broad isotropic diffraction maximum (inset). The HuD connected network (panel C) broadly preserves the  $\mathbf{k}$  space characteristics (panel D) of the point pattern. Sketches and SEM images of the resulting pillar-type (panel E and G) and network-type (panel F and H) metasurfaces.

in Fig. 1G), and *network-type* designs (identical but inverted) consisting of a connected network of gold (sketch in Fig. 1F and SEM in Fig. 1H). The samples are labelled as  $L_p N$  for pillars and  $L_n N$  for networks, with  $N = a \times \sqrt{4000}$ : for example  $L_p 50$  for  $a = 790$  nm has a side dimension of  $50 \mu\text{m}$ . Network designs larger or smaller than  $40 \mu\text{m}$  have been cropped or periodically repeated, respectively, to cover a  $40 \times 40 \mu\text{m}^2$  area.

Fig. 2 presents light scattering experiments on the pillar-type metasurfaces whose SEM images are shown in Fig. 2A. Similar experiments performed on the network-type samples led to comparable results and are not shown here. The measured farfield intensity distribution of each pillar metasurface is shown in Fig. 2B. The samples were illuminated through the glass substrate with a collimated laser ( $\lambda = 532$  nm) while the back-scattered light was

recorded in the farfield by imaging the Fourier plane of a microscope objective (oil immersion, NA=1.45). The maximum observable momenta is overlaid as a coloured dashed circle. All  $L_p 50 - L_p 30$  samples exhibit broad and statistically isotropic scattering rings which resemble the primary resonance of the designed structure factor shown in the inset of Fig. 1D. The momentum associated with the scattering resonance peak increases with the down-scaling of the sample; in  $L_p 25 - L_p 20$  the scattering ring crosses over the observable momentum limit. The bright spot at the centre of each farfield results from the specular reflection along the axis of incidence.

Fig. 2C shows the azimuthally averaged farfield intensity distributions. As the sample correlation length is reduced in size, the momentum of the primary scattering peak increases with a small intensity decrease. The structures  $L_p 50 - L_p 35$  are all characterised by a single scattering peak with some finer structure that varies from sample to sample. Interestingly, the  $L_p 30$  sample exhibits a double peak, while  $L_p 25$  only a secondary low shoulder peak. The linear scaling with the reciprocal of the correlation length, shown in the insets of Figs. 2C, can be expected by simple diffraction theory, while the finer structures are captured by numerical finite-difference time-domain (FDTD) simulations shown in Fig. 2D. In particular, FDTD predicts the multi-peak signature of the  $L_p 30$  sample, suggesting that this feature is a genuine property of the sample. We attribute this finer structure to the interplay of the surface plasmon at the air/gold interface sustained by a single pillar with the linear diffraction dispersion. In fact, the HuD structure comprises elements of different sizes, much larger than the plasmon wavelength, which present high-order resonances in the visible range and an overall response close to that of a surface plasmon resonance of an infinite film which peaks around  $k/k_0 = 1.09$ .

We performed also a broadband scattering characterization of the  $L_p 50$  design. The sample was illuminated from below with white light, and the reflected and scattered light was spectrally decomposed into its wavelength and momentum components (Fig. 3B) by spectrally imaging the Fourier plane of the sample. In this way an energy-wavevector dispersion diagram can be constructed as shown in Fig 3B (experiments) and Fig 3A (FDTD calculations). Both images display a bold diagonal slash, from low-scattering angle to high-scattering angle, and the evolution, for increasing wavelengths, towards larger momenta of the primary scattering peak. From this linear relationship we conclude that the light diffraction follows the designed structure factor with a single main peak (Fig. 1D).

So far, we have investigated the ability of our gold metasurfaces to mediate between incident and scattered light. We now seek to characterise the HuD metasurface electromagnetic modes and their momentum distribution. The metasurface modes are excited

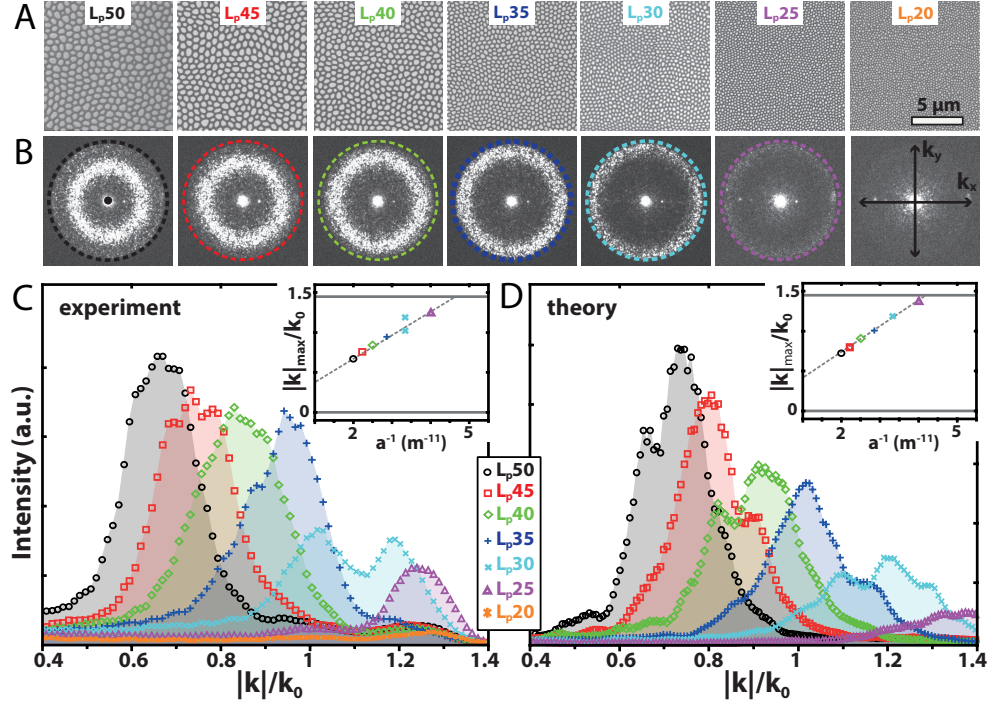


FIG. 2. SEM images of pillar type designs (panel A) together with their farfield diffraction patterns (panel B) when illuminated with a 532 nm laser. The numerical aperture limits are marked as coloured rings. Panel C displays the azimuthally integrated farfields distributions as a function of in-plane momentum (normalized to the incident wavevector  $k_0$ ), showing broad scattering resonances. Panel D shows the same calculated azimuthally integrated farfields which agrees well with experiment. The insets (panel C & D) plots the scattering peak position as a function of the reciprocal scaling parameter ( $a^{-1}$ ) and the expected linear dependence.

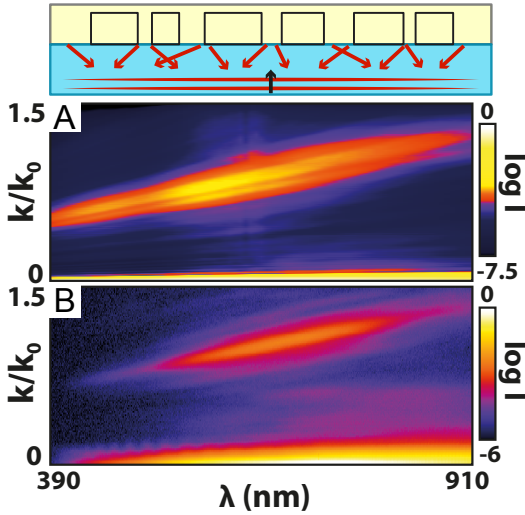


FIG. 3. Theoretical (A) and experimental (B) white light scattering by the  $L_p50$  metasurface. Both theory and experiment match well and show that the scattering peak momentum increases linearly with wavelength.

by a 50 nm layer of Poly(methyl methacrylate) polymer highly doped with fluorescent 4-(Dicyanomethylene)-2-methyl-6-(4-dimethylaminostyryl)-4H-pyran (DCM) dye

molecules which was spin coated on the samples (Fig. 4, top panel). Figs. 4A and B present the theoretical and experimental frequency-momentum distribution, or dispersion plot, of the fluorescence light emitted from the  $L_p50$  structure when excited with a green laser at a wavelength of 532 nm.

The pair of intense emission bands just outside the light lines (white dashed lines indicating  $k/k_0 = \pm 1$ ) results from the characteristic radiation profile of a dipole near the glass-air interface [33]. Inside the light cone, we observe annular features which describe the decomposition of the metasurface slab modes into their in-plane momentum components. These may be viewed as the generalised dispersion relation  $\omega(\mathbf{k})$  of the slab modes. Similar dispersion diagrams were measured for the  $L_p50$ ,  $L_p45$ ,  $L_p40$ ,  $L_p35$  and  $L_p30$  metasurfaces.

In order to further analyse the dispersion plots of Figs. 4, we convert the emission wavelength and in-slab momentum to the dimensionless quantities  $a/\lambda$  and  $ka/2\pi$  respectively. The experimental dispersion diagrams can then be stacked into a single image to illustrate the dispersion over a large normalized frequency range (Fig. 5, left panel). It shows that the fluorescent light is emitted isotropically from the HuD surface, into a cone with varying opening angle, which depends on the emission



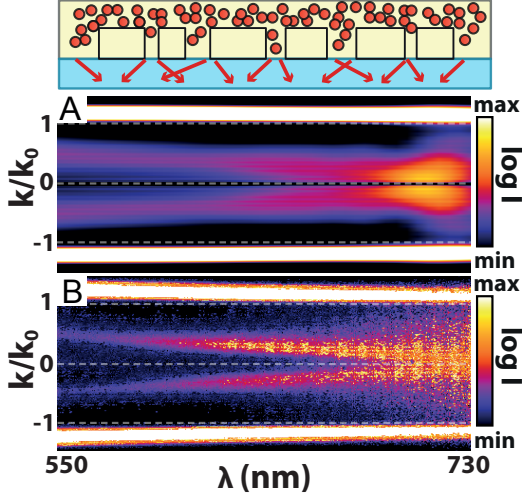


FIG. 4. Generalised dispersion relation  $\omega(k)$  of  $L_p50$  slab modes calculated summing incoherently the farfields of 48 randomly oriented dipole (panel A) and measured by fluorescence emission (panel B).

wavelength to correlation length ratio. As the frequency increases from  $a/\lambda = 0.63$ , the dominant momentum of the slab modes first decreases, reaching a zero in the region of  $a/\lambda = 0.9$ , at which point light is emitted normal to the slab plane, before gradually opening back out. The experiments are in good agreement with FDTD calculations (Fig. 5, right panel) obtained with the spectral function method [32]. Specifically, decomposition of a slab's eigenmodes into a plane wave basis can directly predict the farfield angular profile of its directional emission. These results show that the electromagnetic dispersion diagram of the HuD metasurface follows the designed structure factor (Figure 1D) and exhibits band folding resulting from Bragg-like processes.

In conclusion, we designed, fabricated and characterized gold metasurfaces derived from HuD connected networks. By reciprocal space engineering we designed the structure factor to be dominated by a single, broad scattering resonance which was observed to dictate both the annular farfield light scattering and directional emission properties of the metasurfaces. The observed HuD metasurface dispersion corresponds to an effective medium band that is back-folded by Bragg-like processes. Surface plasmon resonance where found to contribute to the diffraction by inducing additional peaks from their interaction with the structural diffraction peak. The observed light emission and scattering engineering has important applications for light extraction from light-emitting devices, absorption in solar cells and annular redirection for displays, by exploiting the full azimuthal symmetry provided by the HuD metasurfaces design.

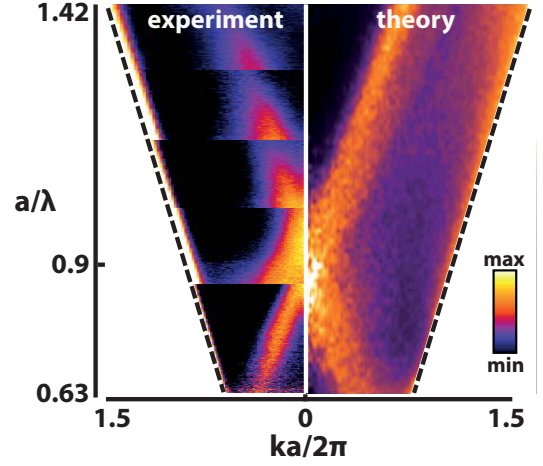


FIG. 5. Left, experimental dispersion relations for samples  $L_p50$ ,  $L_p45$ ,  $L_p40$ ,  $L_p35$  and  $L_p30$  are stacked together as a function of  $a/\lambda$ . Right panel, FDTD simulations which confirm the crossing at  $a/\lambda = 0.9$  where the light is emitted normal to the metasurface plane.

#### ACKNOWLEDGEMENTS

The work was supported by the Engineering and Physical Sciences Research Council (EPSRC EP/M027961/1 and EP/M013812/1), the Leverhulme Trust (RPG-2014-238) and the Royal Society (RG140457).

\* [m.florescu@surrey.ac.uk](mailto:m.florescu@surrey.ac.uk)

† [riccardo.sapienza@kcl.ac.uk](mailto:riccardo.sapienza@kcl.ac.uk)

- [1] Behrad Gholipour, Jianfa Zhang, Kevin F. MacDonald, Daniel W. Hewak, and Nikolay I. Zheludev, "An all-optical, non-volatile, bidirectional, phase-change meta-switch," *Adv. Mater.* **25**, 3050–3054 (2013).
- [2] P Hosseini, C D Wright, and H Bhaskaran, "An optoelectronic framework enabled by low-dimensional phase-change films," *Nature* **511**, 206–211 (2014).
- [3] Abul K Azad, Wilton J M Kort-Kamp, Milan Sykora, Nina R Weisse-Bernstein, Ting S Luk, Antoinette J Taylor, Diego A R Dalvit, and Hou-Tong Chen, "Metasurface Broadband Solar Absorber." *Sci. Rep.* **6**, 20347 (2016).
- [4] Thamer S. Almongeeef and Omar M. Ramahi, "Metamaterial electromagnetic energy harvester with near unity efficiency," *Appl. Phys. Lett.* **106** (2015), 10.1063/1.4916232.
- [5] W. L. Barnes, T. W. Preist, S. C. Kitson, J. R. Sambles, N. P K Cotter, and D. J. Nash, "Photonic gaps in the dispersion of surface plasmons on gratings," *Phys. Rev. B* **51**, 11164–11167 (1995).
- [6] J-S Bouillard, P Segovia, W Dickson, G a Wurtz, and a V Zayats, "Shaping plasmon beams via the controlled illumination of finite-size plasmonic crystals." *Sci. Rep.* **4**, 7234 (2014).

- [7] V. Giannini, G. Vecchi, and J. Gómez Rivas, “Lighting up multipolar surface plasmon polaritons by collective resonances in arrays of nanoantennas,” *Phys. Rev. Lett.* **105**, 266801 (2010).
- [8] L. Dal Negro and S. V. Boriskina, “Deterministic aperiodic nanostructures for photonics and plasmonics applications,” *Laser Photonics Rev.* **6**, 178–218 (2012).
- [9] Steven M. Lubin, Alexander J. Hryn, Mark D. Huntington, Clifford J. Engel, and Teri W. Odom, “Quasiperiodic moiré plasmonic crystals,” *ACS Nano* **7**, 11035–11042 (2013).
- [10] Nate Lawrence, Jacob Trevino, and Luca Dal Negro, “Aperiodic arrays of active nanopillars for radiation engineering,” *J. Appl. Phys.* **111** (2012), 10.1063/1.4723564.
- [11] Farzaneh Afshinmanesh, Alberto G. Curto, Kaveh M. Milaninia, Niek F. Van Hulst, and Mark L. Brongersma, “Transparent metallic fractal electrodes for semiconductor devices,” *Nano Lett.* **14**, 5068–5074 (2014).
- [12] Michele Gaio, Marta Castro-Lopez, Jan Renger, Niek van Hulst, and Riccardo Sapienza, “Percolating plasmonic networks for light emission control,” *Faraday Discuss.* **178**, 237–252 (2015).
- [13] A. Hinke Schokker and A. Femius Koenderink, “Statistics of randomized plasmonic lattice lasers,” *ACS Photonics* **2**, 1289–1297 (2015).
- [14] R. Zhang, S. Knitter, S. F. Liew, F. G. Omenetto, B. M. Reinhard, H. Cao, and L. Dal Negro, “Plasmon-enhanced random lasing in bio-compatible networks of cellulose nanofibers,” *Appl. Phys. Lett.* **108** (2016), 10.1063/1.4939263.
- [15] Nanfang Yu, Patrice Genevet, Mikhail A Kats, Francesco Aieta, Jean-Philippe Tetienne, Federico Capasso, and Zeno Gaburro, “Light propagation with phase discontinuities: generalized laws of reflection and refraction,” *Science* **334**, 333–7 (2011).
- [16] Xingjie Ni, Alexander V Kildishev, and Vladimir M Shalaev, “Metasurface holograms for visible light,” *Nat. Commun.* **4**, 2807 (2013).
- [17] Emiliano R Martins, Juntao Li, YiKun Liu, Valérie Depauw, Zhanxu Chen, Jianying Zhou, and Thomas F Krauss, “Deterministic quasi-random nanostructures for photon control,” *Nat. Commun.* **4**, 2665 (2013).
- [18] Matteo Burresi, Filippo Pratesi, Kevin Vynck, Mauro Prasciolu, Massimo Tormen, and Diederik S. Wiersma, “Two-dimensional disorder for broadband, omnidirectional and polarization-insensitive absorption,” *Opt. Express* **21**, A268–A275 (2013).
- [19] Ad Lagendijk, Bart Van Tiggelen, and Diederik S. Wiersma, “Fifty years of Anderson localization,” *Phys. Today* **62**, 24–29 (2009).
- [20] Won Hoe Koo, Soon Moon Jeong, Fumito Araoka, Ken Ishikawa, Suzushi Nishimura, Takehiro Toyooka, and Hideo Takezoe, “Light extraction from organic light-emitting diodes enhanced by spontaneously formed buckles,” *Nat. Photonics* **4**, 222–226 (2010).
- [21] Luis S. Froufe-Pérez, Michael Engel, Pablo F. Damasceno, Nicolas Muller, Jakub Haberko, Sharon C. Glotzer, and Frank Scheffold, “Role of short-range order and hyperuniformity in the formation of band gaps in disordered photonic materials,” *Phys. Rev. Lett.* **117**, 053902 (2016).
- [22] Marian Florescu, Salvatore Torquato, and Paul J Steinhardt, “Designer disordered materials with large, complete photonic band gaps,” *Proc. Natl. Acad. Sci.* **106**, 20658–20663 (2009).
- [23] Marian Florescu, Salvatore Torquato, and Paul J. Steinhardt, “Complete band gaps in two-dimensional photonic quasicrystals,” *Phys. Rev. B - Condens. Matter Mater. Phys.* **80** (2009), 10.1103/PhysRevB.80.155112.
- [24] Nicolas Muller, Jakub Haberko, Catherine Marichy, and Frank Scheffold, “Silicon hyperuniform disordered photonic materials with a pronounced gap in the shortwave infrared,” *Adv. Opt. Mater.* **2**, 115–119 (2014).
- [25] Weining Man, Marian Florescu, Eric Paul Williamson, Yingquan He, Seyed Reza Hashemizad, Brian Y C Leung, Devin Robert Liner, Salvatore Torquato, Paul M Chaikin, and Paul J Steinhardt, “Isotropic band gaps and freeform waveguides observed in hyperuniform disordered photonic solids,” *Proc. Natl. Acad. Sci.* **110**, 15886–15891 (2013).
- [26] Wen Zhou, Zhenzhou Cheng, Bingqing Zhu, Xiankai Sun, and Hon Ki Tsang, “Hyperuniform Disordered Network Polarizers,” *IEEE J. Sel. Top. Quantum Electron.* **22**, 288–294 (2016).
- [27] R. Degl’Innocenti, Y. D. Shah, L. Masini, A. Ronzani, A. Pitanti, Y. Ren, D. S. Jessop, A. Tredicucci, H. E. Beere, and D. A. Ritchie, “Hyperuniform disordered terahertz quantum cascade laser,” *Sci. Rep.* **6**, 19325 (2016).
- [28] C. De Rosa, F. Auriemma, C. Diletto, R. Di Girolamo, a. Malafronte, P. Morvillo, G. Zito, G. Rusciano, G. Pesce, and a. Sasso, “Toward hyperuniform disordered plasmonic nanostructures for reproducible surface-enhanced Raman spectroscopy,” *Phys. Chem. Chem. Phys.* **17**, 8061–8069 (2015).
- [29] O. Leseur, R. Pierrat, and R. Carminati, “High-density hyperuniform materials can be transparent,” *Optica* **3**, 763 (2016).
- [30] Marian Florescu, Paul J. Steinhardt, and Salvatore Torquato, “Optical cavities and waveguides in hyperuniform disordered photonic solids,” *Phys. Rev. B* **87**, 165116 (2013).
- [31] Timothy Amoah and Marian Florescu, “High-Q optical cavities in hyperuniform disordered materials,” *Phys. Rev. B* **91**, 020201 (2015), arXiv:1504.07055.
- [32] Samuel Tsitrin, Eric Paul Williamson, Timothy Amoah, Geev Nahal, Ho Leung Chan, Marian Florescu, and Weining Man, “Unfolding the band structure of non-crystalline photonic band gap materials,” *Sci. Rep.* **5**, 13301 (2015).
- [33] Lukas Novotny, *Principles of Nano-Optics* (Cambridge University Press, Cambridge, UK, 2006) arXiv:arXiv:1011.1669v3.